ENGINEERING TRANSACTIONS • *Engng. Trans.* • **39**, 1, 75–96, 1991
Polish Academy of Sciences • Institute of Fundamental Technological Research

ON THE KINEMATICALLY ADMISSIBLE SOLUTION APPLIED TO THE THEORETICAL ANALYSIS OF SHOVING PROCESSES

W. TRĄMPCZYŃSKI and A. JARZĘBOWSKI
(WARSZAWA)

The paper concerns a simplified theoretical analysis of such complex soil shoving processes as, for example, the process of moving walls in a way similar to heavy machine tools (e.g. bucket of a loading machine). Assuming the material to be rigid-perfectly plastic with strain behaviour governed by the Coulomb–Mohr yield criterion and associated flow rule, simple kinematically admissible solutions were found. It was shown that, using this technique step by step, it was possible to analyse complex processes and even to find more effective loading paths.

1. INTRODUCTION

The problem of passive and active pressures exerted by a granular medium on a rigid wall under plane strain conditions has often been analysed in numerous works. Several theoretical solutions were obtained within the theory of plasticity under the assumption of the rigid-perfectly plastic behaviour of a granular material [1, 2, 3]. Quite often the method of characteristics was used to solve static and kinematic equations [1]. Although a number of boundary value problems were solved in this way, there exist several limitations in obtaining complete solutions or even kinematically admissible solutions. The applicability of this technique to the analysis of soil shoving problems was discussed in [4, 5]. It was shown that, apart from other limitations, limitations concerning the shape of a free boundary practically restrict possible solutions (complete and kinematic ones) only to the incipient motion and convex free boundaries. So it is not possible to follow in this way

more complex processes as, for example, the process of moving walls in a way similar to such heavy machine tools as bulldozer blades or loader buckets. Since a theoretical description of such processes can have great practical importance, in this paper another simplified technique was used to describe it. Assuming the rigid-perfectly plastic behaviour of a material and the associated flow rule, kinematically admissible mechanisms for such a process were studied. According to the limit load theorems [3], such solutions give only the upper bound for forces necessary for the realization of such a process. As it was shown in [6], using only three typical kinds of mechanisms, solutions very close to complete ones and statically admissible ones could be obtained in this way. So it can be assumed that such kinematically admissible solutions can give a rather good estimation of real processes. In the present paper the process of the wall shaped similarly to the bucket of the loading machine, with motions in a way similar to loading machine tools, was studied.

The proposed solutions were obtained under the assumption of the rigid-perfectly plastic material behaviour coupled with the associated flow rule. In several papers [7, 8, 9] it was shown that the associated flow rule for the Coulomb–Mohr material is not a good approximation of the real material behaviour (experiments were performed mainly on sand). It also concerns the dilatation effect, which is overstimated by this theory, as well as the calculated plastic zone range. So the non-associated flow rules should be used for proper material description. Also, the assumption of material rigid-perfectly plastic behaviour reflects real behaviour only in a broad qualitative sense [10].

Thus, the results obtained in the way presented in this paper should be treated as qualitative ones, and as such will be compared (in the future) with experimental data. It should be emphasized, that there does not exist now any other simple method to follow such complicated processes as the ones considered.

2. Kinematically admissible solutions for wall pressure problems

Let us assume the material to be rigid-perfectly plastic and the plastic strain to obey the modified Coulomb–Mohr yield criterion, where

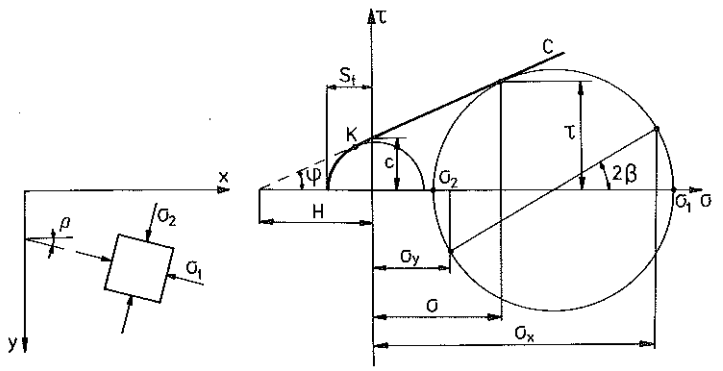

Fig. 1. The modified Coulomb-Mohr yield criterion for plane strain conditions in the $\sigma - \tau$ axes.

its linear part (Fig.1–KC) is described by the following equations:

$$(\sigma_x - \sigma_y)^2 + 4\tau_{xy}^2 = (\sigma_x + \sigma_y + 2H)^2 \sin^2\varphi, \qquad H = c \cdot \operatorname{ctg}\varphi,$$

(2.1)

$$|\tau| = c + \sigma \operatorname{tg}\varphi,$$

with material strength subject to uniform extension limited to S_t [11], where c – material cohesion parameter, φ – internal friction angle;

the associated flow rule takes the form

(2.2)
$$\dot{\varepsilon}_{ij} = \dot{\lambda}\frac{\partial F}{\partial \sigma_{ij}}.$$

According to the limit load theorems [3], any statically admissible solution defines the lower bound of the limit load and any kinematically admissible one defines the upper bound. So, if it is not possible to find complete solutions of a certain problem, one can try to find the upper or the lower bound of the limit load (or both). If the difference between such two solutions (kinematic and static ones) is not too large, a good estimation of the complete solution may be found.

In the present paper the kinematically admissible solutions for a process similar to that of filling a bucket of a loading machine were studied. By kinematically admissible, we mean an arbitrary solution satisfying all kinematic constraints and the positive dissipation energy equation

(2.3)
$$\sigma_{ij} \cdot \dot{\varepsilon}_{ij} \geq 0$$

in all points of the field under consideration.

Let us discuss the problem of the wall pressure shown in Fig.2.

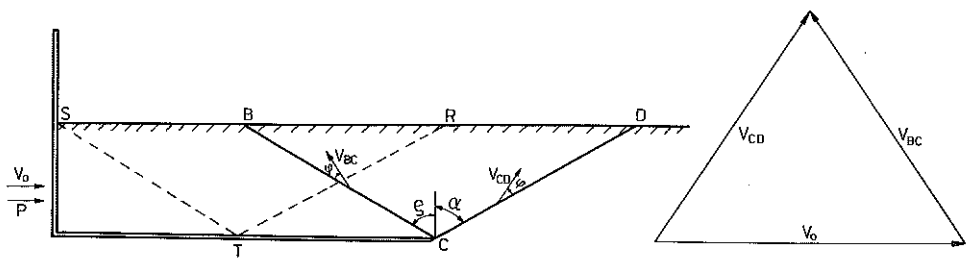

Fig. 2. The rigid wall (shaped similar to the bucket of a loading machine) pressure problem and its kinematically admissible solution.

A simple kinematically admissible mechanism consists of rigid triangle ΔBCD motion along the slip lines CD and BC. The force value P necessary to realize the incipient motion can be determined from the following energy dissipation equation:

$$P \times V_0 = D_{CD} + D_{BC} + D_G, \tag{2.4}$$

where D_{CD} – energy dissipated along the slip line CD, D_{BC} – energy dissipated along the slip line BC, D_G – energy dissipated in the process of rigid triangle ΔBCD lifting (for $\gamma \neq 0$).

It is possible to show [3], that for the associated flow rule (2.2) and modified Coulomb–Mohr yield criterion $(2.1)_2$ the velocity vector along a slip line is inclined by an angle φ to this line and the energy dissipation per unit length along the slip lines (as CD and CB) can be described by the following equation:

$$D_L = c \times \cos\varphi \times V_L, \tag{2.5}$$

where V_L – velocity vector along the slip line (Fig.2 – V_{BC}, V_{CD}). Energy dissipation due to gravity forces can be expressed in the form

$$D_G = V_G \times G, \tag{2.6}$$

where G – ΔBCD weight, V_G – lifting velocity. So the P (upper bound) value can be determined from the equation

$$P \times V_0 = c \times \cos\varphi \times V_{CD} \times CD + c \times \cos\varphi \times V_{BC} \times BC + G \times V_G. \tag{2.7}$$

Kinematically admissible solutions for the incipient motion of different wall shapes were discussed in [6]. It was shown that using only three

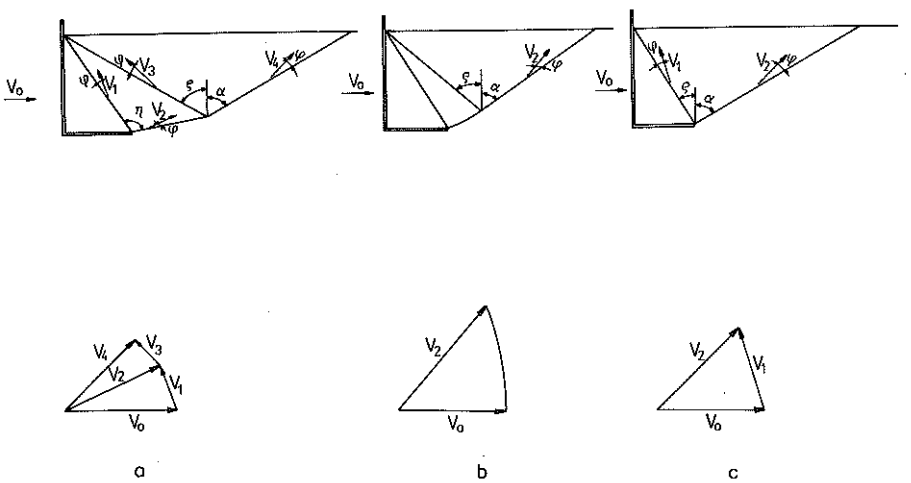

Fig. 3. Kinematically admissible solution of the rigid wall pressure problems for different wall shapes.

simple mechanisms (Fig.3a – four slip lines solution, Fig.3b – solution

with logarithmic line, Fig.3c – two slip lines solution) for walls shaped similarly to heavy machine tools, solutions close to complete ones and kinematically admissible ones (assuming the associated flow rule) could be obtained.

A wide discussion of kinematically admissible solutions applied to earth moving processes was presented in [12].

3. Soil shoving process by a rigid wall shaped similarly to the bucket of a loading machine-theoretical description

3.1. Solutions for the material obeying the Coulomb–Mohr yield criterion

Let us discuss the process shown schematically in Fig.4. It can be

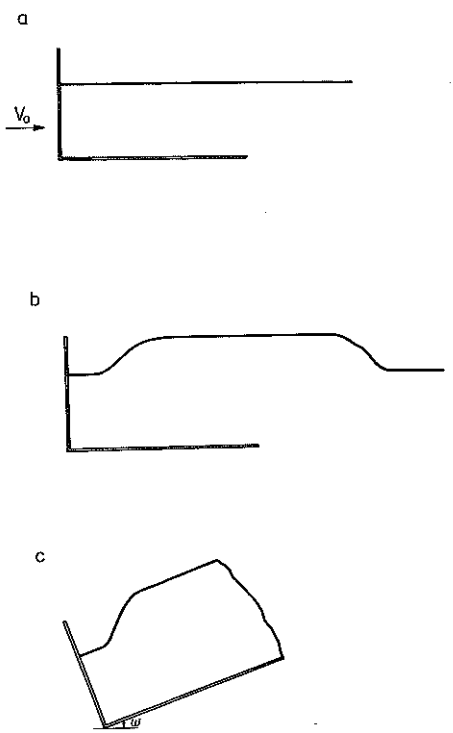

Fig. 4. A model for the loading machine working process.

considered to be a model for a working process of the bucket of a loading machine. Two basic phases could be distinguished: 1) the tool pushing phase (Fig.4a,b), 2) the tool filling phase (Fig.4c). At the beginning, the problem shown in Fig.2 has to be solved. Assuming the material to be rigid-perfectly plastic with the plastic behaviour governed by a) modified Coulomb-Mohr yield criterion (Fig.1) and b) associated flow rule (2.2), energetically most efficient solution was searched. Kinematically admissible solutions were limited to the types schematically shown in Fig.3.

The incipient tool motion can be described by a simple solution with two lines (Fig.2), which is energetically most efficient (the lowest pushing force was obtained). Although processes based on different slip line position are just as efficient energetically (for example the dashed lines ST and TR in Fig.2), only slip lines starting from the tool were experimentally observed [4]. Optimal slip line inclinations (α and ρ values) were searched for at every moment of the process. In the case shown in Fig.2 they are $\alpha = \rho = 57°$. For the material described by the following parameters [13]: $c = 19.6$ kPa, $\varphi = 26°$, $\gamma = 19.6$ kN/m^3 the situation after displacement U_0 is shown in Fig.8. The rigid triangle ΔBCD has moved to a new position $\Delta B''C''D''$. Because of sliding along the slip lines, the regions 2 and 3 contain a material with density different from the virgin one 1. This is due to the fact that for the associated flow rule, two processes having an influence on the material parameters appear on the slip lines: dilatation and shear. In order to describe such an influence, two different parameters were introduced:

for the dilatation – parameter $\overset{*}{U}_n$:

$$\overset{*}{U}_n = \int dU_n, \tag{3.1}_1$$

for the shear – nondiminishing parameter U_s:

$$\overset{*}{U}_s = \int |dU_s|, \tag{3.1}_2$$

where dU_n and dU_s were defined according to the corresponding displacements dn and ds (Fig.5), where b_0 is thickness of the material layer cut at each single linear step of the process. It follows from geometrical considerations that the first process influences density according to following equation:

$$\gamma = \frac{\gamma_0}{\overset{*}{U}_n + 1}, \tag{3.2}$$

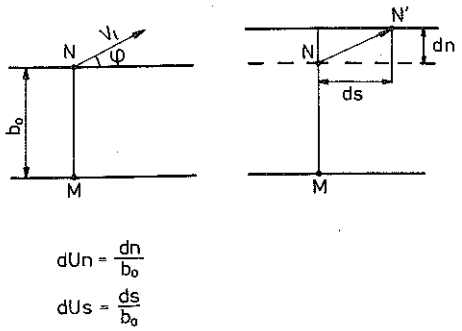

Fig. 5. Dilatation and shear processes on a slip line in the case of the associated flow rule assumption.

where γ_0 denotes density of the virgin material. It was assumed that the second one influences material cohesion c (in the Coulomb–Mohr yield criterion) according to the following assumed relation [14]:

$$c = (c_0 - c_R) \times \exp(-\overset{*}{U}_s \times A) + c_R, \tag{3.3}$$

where c_0 – cohesion of the virgin material, c_R – residual cohesion value, A – material constant.

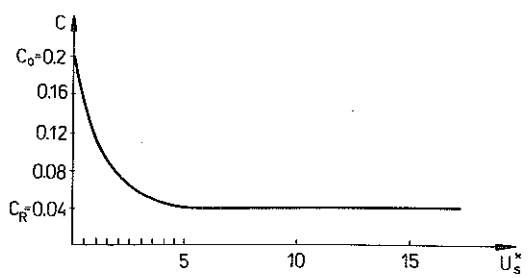

Fig. 6. The material cohesion parameter c.

Relation c versus $\overset{*}{U}_s$ was graphically shown in Fig.6 for the following parameters: $c_0 = 19.6$ kPa, $c_R = 3.92$ kPa, $A = 0.8$, assumed for the considered material.

Similarly, tensile strength of the material subject to uniform extension S_t is also assumed to decrease according to the relation

$$S_t = (S_{t_0} - S_{tR}) \times \exp(-\overset{*}{U}_s \times A) + S_{tR}, \tag{3.4}$$

where S_{t_0} and S_{tR} are its initial and residual values. They were assumed to be, respectively, 14.7 and 2.94 kPa. Let us assume that the process shown in Fig.2 is carried on step by step with the unit displacement U (Fig.7). Then, the parameters $\overset{*}{U}_n$ and $\overset{*}{U}_s$ are given by the following

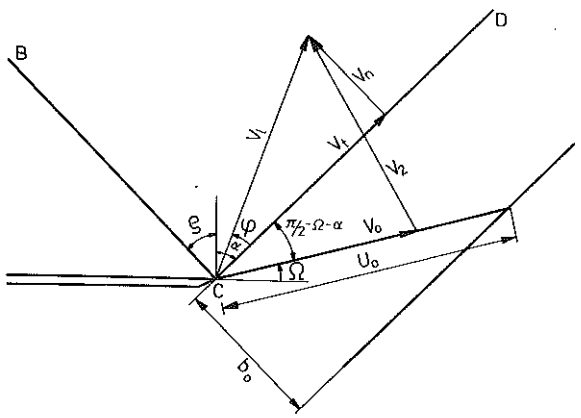

Fig. 7. The material velocity on the tool edge.

equations (see Fig.7):

$$dU_n^{CD} = \frac{\sin\varphi\,\cos(\rho-\varphi)}{\cos\alpha\,\sin(\alpha+\rho-2\varphi)},$$

(3.5)

$$dU_s^{CD} = \frac{\cos\varphi\,\cos(\rho-\varphi)}{\cos\alpha\,\sin(\alpha+\rho-2\varphi)},$$

and for the slip line BC:

$$dU_n^{BC} = \frac{\cos(\alpha+\Omega-\varphi)\,\sin\varphi}{\cos\alpha\,\sin(\alpha+\rho-2\varphi)},$$

(3.6)

$$dU_s^{BC} = \frac{\cos(\alpha+\Omega-\varphi)\,\cos\varphi}{\cos\alpha\,\sin(\alpha+\rho-2\varphi)}.$$

It is worth to mention that for the DC line, after every unit displacement the slip line is realized within a "new" (virgin) material. In the case of the BC line the same material shears and dilatates all the time.

Let us consider several subsequent steps of the pushing process, all with the constant lateral displacement U_0 , limiting the types of kinematically admissible solution to that shown in Fig.3.

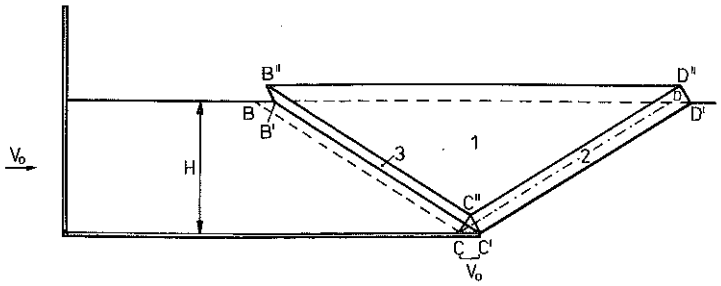

Fig. 8. The kinematically admissible solution at a certain stage of the rigid wall pressure process (first step).

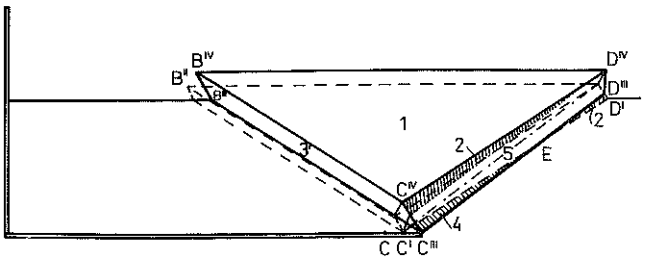

Fig. 9. The kinematically admissible solution at a certain stage of the rigid wall pressue process.

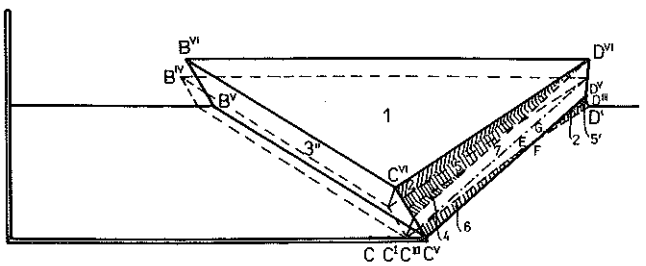

Fig. 10. The kinematically admissible solution at a certain stage of the rigid wall pressure process.

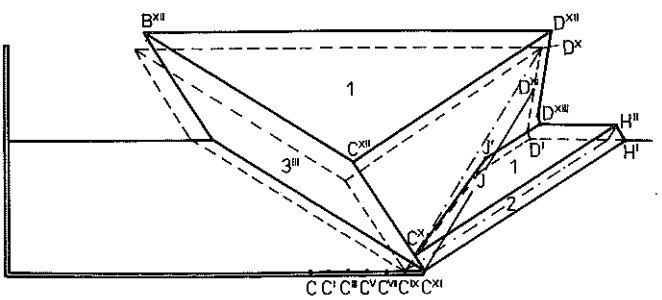

Fig. 11. The kinematically admissible solution at a certain stage of the rigid wall pressure process (advanced tool displacement).

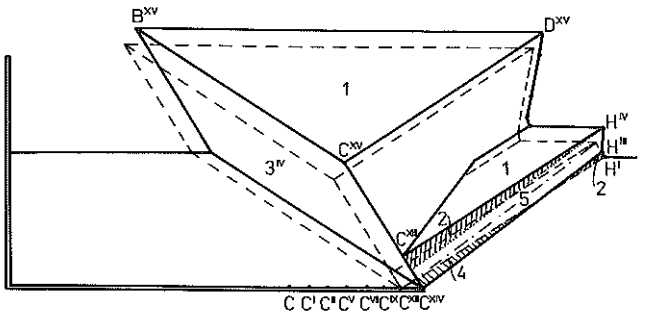

Fig. 12. The kinematically admissible solution at a certain stage of the rigid wall pressure process (after advanced tool displacement).

Some following phases are shown in Figs.8–12 (it was found that the mechanism shown in Fig.2 was energetically most effective during the entire process considered).

The soil shape after the step was marked with solid lines in each of the figures and before the step with dashed lines. Assume that during each step slip lines translate parallely through the material (for example from position CD to $C'D'$ in Fig.8). The front of the CD slip line before each step was marked with a dotted line. Using the same kinematically addmissible mechanism, new positions of the slip lines (α and ρ values) were searched for after each step of the process referring to the minimum energy value (Eq.(2.7)). Nonetheless, while searching for the minimum value of the right side of Eq.(2.7), the positions of the slip lines following the increment step were used (cf. Figs.9–12). The total thickness of the cut layer was assumed to be (Fig.8) $H = 35$cm. The CD slip line direction changes during the process (the α value increases) while the BC slip line direction remains constant (compare $C'D'$, $C'''D'''$ and $C^{\mathrm{V}}D^{\mathrm{V}}$ lines and $B'C'$, $B'''C'''$ and $B^{\mathrm{V}}C^{\mathrm{V}}$ lines in Figs.8–10). Such a process produces different material zones with different material parameter values. This was taken into account while searching for optimal slip line positions after each step. For example, after the third step (Fig.10) one can distinguish seven zones:

$$\begin{aligned} 1 &: c_1 = 19.6\ [\mathrm{kPa}]: & S_{t1} &= 14.7\ [\mathrm{kPa}]\ , \\ 2 &: c_2 = 4.41 & S_{t2} &= 3.33\ , \\ 3 &: c_3 = 3.94 & S_{t3} &= 2.95\ , \end{aligned}$$

$$\begin{aligned} 4 : c_4 &= 4.31 \qquad S_{t4} = 3.23\,, \\ 5 \cong 5' : c_5 &= 3.93 \qquad S_{t5} = 2.94\,, \\ 6 : c_6 &= 4.30 \qquad S_{t6} = 3.22\,, \\ 7 : c_7 &= 3.92 \qquad S_{t7} = 2.94\,. \end{aligned}$$

Slip line CD changes its orientation into a more and more vertical one to reach the step shown in Fig.11 when the slip line position $C^{XI}H'$ turns out to be energetically more efficient than the position $C^{XI}D^{XI}$. From this moment the process starts to be nearly periodically repeatable (it would be fully repeatable for the weightless material) – the second step is similar to the first one, the next step to the second one (compare Figs.11 and 8, and 12 and 9). Zone $C^{X}J'D^{XIII}H''$ consists of the virgin material, like triangle $\Delta B^{XII}C^{XII}D^{XII}$ (Fig.11). Zone $C^{X}J'D^{XIII}D^{XII}C^{XII}$ consists of several zones with different material parameters what, for simplicity, was not indicated in Figs.11 and 12. Of course, in the real process the CD slip line position would change smoothly at the beginning (simultaneous translation and rotation) to jump rapidly into the new position after some horizontal tool displacement. In any case the characteristic scale - shaped rigid zones generated during cohesive soil cutting can be described using the presented model.

In Sect. 3.2 of this paper a similar solution for the material obeying the Tresca yield criterion was presented.

As it can be observed in Fig.8, the wedge $B'B''D''$ is pushed out during the pushing phase. It can slide down as a result of several mechanisms. Three of them are shown in Fig.13. In the first case it was assumed that the slip occurs along the slip line $B'E$ (Fig.13a). Comparing the energy disspation, the h value necessary to realize such a process can be calculated:

$$V_G \times G_1 + V_G \times G_3 = V \times \cos\varphi \times c_1 \times FE + V \times \cos\varphi \times c_3 \times B'F, \tag{3.7}$$

$$\begin{aligned} h = \Bigg(\cos\varphi \Bigg[c_1 \left(\frac{1}{\cos\alpha} - \frac{\sin\varphi}{\cos(\rho-\varphi)\sin(\alpha+\rho)}\right) \\ + c_3 \frac{\sin\varphi}{\cos(\rho-\varphi)\sin(\alpha+\rho)}\Bigg]\Bigg) \Big/ \Bigg(\cos(\alpha+\varphi) \cdot \frac{1}{2} \cdot \frac{\sin(\alpha+\rho-\varphi)}{\sin(\alpha+\rho)} \cdot \frac{1}{\cos(\rho-\varphi)} \\ \times \left[\frac{\sin(\alpha+\rho-\varphi)\cos\rho}{\cos\alpha\cos(\rho-\varphi)} \cdot \gamma_1 + \frac{\sin\varphi}{\cos(\rho-\varphi)} \cdot \gamma_3\right]\Bigg). \end{aligned} \tag{3.8}$$

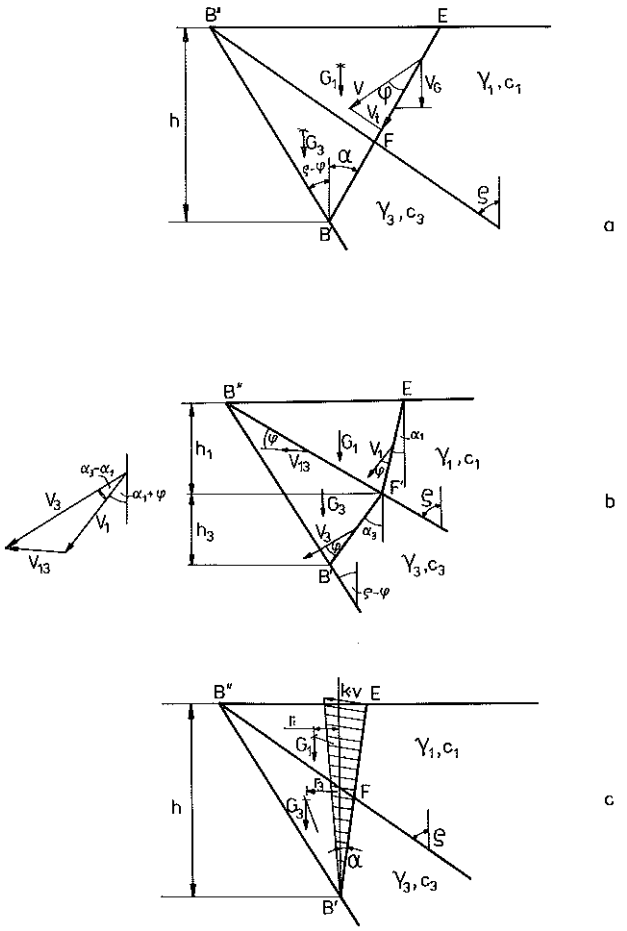

Fig. 13. Different mechanisms for the soil wedge sliding process.

In the second case it was assumed, that the slip line $B'FE$ in not a straight one and an additional slip line $B''F'$ occurs during material sliding. The kinematically admissible mechanism and the velocity hodograph for such a case are shown in Fig.13b. The regions $B'B''F'$ and $B''EF'$ consist of materials with different parameters. From the energy dissipation equation

$$(3.9) \qquad V_{G1} \times G_1 + V_{G3} \times G_3 = V_1 \times \cos\varphi \times c_1 \times EF' + V_3 \times \cos\varphi \times c_3 \times F'B' + V_{13} \times \cos\varphi \times c_3 \times F'B''$$

according to some simple geometrical formulas, one obtains

$$(3.10)\quad h = 2\cos\varphi\left\{\frac{c_1}{\cos\alpha_1}+\frac{c_3\cos(\alpha_3-\alpha_1-\rho-\varphi)}{\cos(\rho-\varphi)}\left[\frac{1}{B\cos\alpha_3}+\frac{\sin(\alpha_3-\alpha_1)}{\cos\rho\cos(\alpha_3-\alpha_1-\rho-\varphi)}\right]\right\}\Big/\left[\cos(\alpha_1+\varphi)(\operatorname{tg}\alpha_1+\operatorname{tg}\rho)\frac{B}{B+1}\gamma_1+\cos(\alpha_3+\varphi)(\operatorname{tg}\alpha_3+\operatorname{tg}\rho)\frac{\cos(\alpha_3-\alpha_1-\rho-\varphi)}{(B+1)\cos(\rho+\varphi)}\gamma_3\right],$$

where α_1 and α_2 are the slip lines position angles (cf. Fig.13b), and the wedge height h is calculated as a sum of h_1 and h_3. Its minimum value turns out to be for $\alpha_1 = \alpha_3 = 19°$. This means that the mechanism concerned translates into the previous one with the straight slip line $B'FE$. The values h calculated from these two mechanisms (Eqs.(3.8) and (3.10)) are equal, and for typical material parameters for clays [13] they exceed standard tool height for such a solution.

The third mechanism (Fig.13c) is assumed to be a rigid material rotation around point B'. The wedge size, described by the h value, can be determined from the following energy equation:

$$(3.11)\quad (G_1\times r_1 + G_2\times r_2)\times\omega = \big(0.5\times(B'F)^2\times S_{t3} + 0.5\times (B'E)^2\times S_{t1} - 0.5\cdot(B'F)^2\times S_{t1}\big)\times\omega,$$

where ω - rotation velocity.

Thus

$$(3.12)\quad h = \left(\frac{1}{2}\left(\frac{\sin\varphi}{\cos(\rho-\varphi)\sin(\alpha+\rho)}\right)^2(S_{t3}-S_{t1}) + \frac{1}{2}\left(\frac{1}{\cos\alpha}\right)^2 S_{t1}\right)\Big/\left[\left(\frac{1}{2}\cdot\frac{(\sin(\alpha+\rho-\varphi))^2}{(\cos(\rho-\varphi))^2}\cdot\frac{\cos\rho\cdot\gamma_1}{\sin(\alpha+\rho)\cos\alpha}\right)\cdot\left\{\left(h\operatorname{tg}(\rho-\varphi)+\left[\frac{\sin\varphi}{\cos(\rho-\varphi)\sin(\alpha+\rho)}+\frac{1}{2}\left(\frac{1}{\cos\alpha}-\frac{\sin\varphi}{\cos(\rho-\varphi)\sin(\alpha+\rho)}\right)\right]\sin\alpha\right)/3-\left[\frac{\sin\varphi}{\cos(\rho-\varphi)\sin(\alpha+\rho)}+\frac{1}{2}\left(\frac{1}{\cos\alpha}-\frac{\sin\varphi}{\cos(\rho-\varphi)\sin(\alpha+\rho)}\right)\right]\sin\alpha\right\}$$

(3.12)
[cont.]

$$+\frac{1}{2}\frac{\sin(\alpha+\rho-\varphi)\sin\varphi\cdot\gamma_2}{(\cos(\rho-\varphi))^2\sin(\alpha+\rho)}\cdot\left\{\left(h\mathrm{tg}(\rho-\varphi)+\frac{1}{2}\frac{\sin\varphi\sin\alpha}{\cos(\rho-\varphi)\sin(\alpha+\rho)}\right)\right.$$
$$\left./\,3-\frac{1}{2}\frac{\sin\varphi-\sin\alpha}{\cos(\rho-\varphi)\sin(\alpha+\rho)}\right\}\Bigg].$$

In that case $h_{\min}$ is comparable with that for previous solutions. None of the sliding down processes mentioned before can occur. Let us stop the tool pushing phase at the moment shown in Fig.12. In general the filling process can be realized basically in two ways:

a) as tool rotation around point O,

b) as tool rotation around point C

(as there is a material under the bucket, this is impossible in the case when horizontal motion of the bucket occured before).

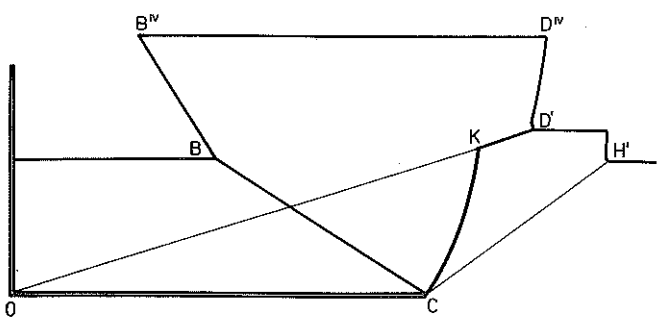

Fig. 14. The kinematically admissible solution for the tool rotation process.

In the first case (Fig.14) the stiff block OKC rotation (KC – logarithmic discontinuity line) and material tear along line KD' are realized. A theoretical description of the first process was given in [3]. For material rotation around point O (Fig.15) the discontinuity vector V is perpendicular to the radius r, and the slip line AB is inclined to this vector by an angle φ. Hence the discontinuity line AB is a logarithmic curve (for $\varphi = 0$ - circle) described by the equation

$$r = r_0 \times \exp(\Theta\tan\varphi), \tag{3.13}$$

and the velocity discontinuity V_{12} is defined by the relation

$$V_{12} = V_{12}^0 \times \exp(\Theta\tan\varphi). \tag{3.14}$$

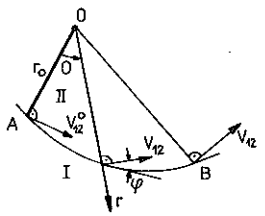

Fig. 15. The kinematically admissible mechanism for the stiff wall rotation process.

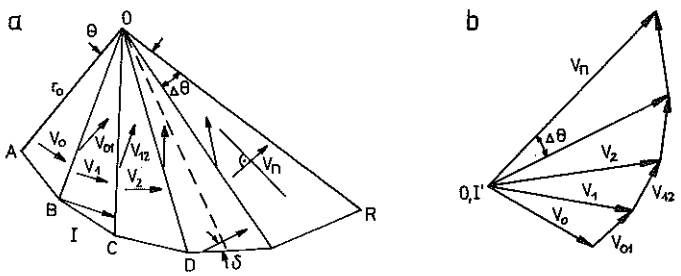

Fig. 16. The kinematically admissible mechanism for the stiff wall rotation process.

Let us discuss a strain process shown in Fig.16a. It consists of n-rigid blocks (OAB, OBC, OCD,...) moving with constant velocities and sliding on each other along the discontinuity lines OB, OC, OD... and AB, BC, CD,... . The velocity hodograph in such a case is shown in Fig.16b. For $n \to \infty$

$$V = V_0 \times \exp(\Theta \tan\varphi). \tag{3.15}$$

Energy dissipated along the slip lines

for OC...

$$D_{OC} = c \times r_2 \times V_1 \times \Delta\Theta \tag{3.16}$$

and for BC...

$$D_{BC} = c \times \left(\frac{r_2 \cdot \Delta\Theta}{\cos\varphi}\right) V_1 \cdot \cos\varphi, \tag{3.17}$$

and, integrating Eq.(3.17) along the logarithmic curve AR ($r = r_0 \exp\theta \operatorname{tg}\varphi$),

$$D_{AOR} = D_{AR} = 0.5 \times c \times V_0 \times r_0 \times \operatorname{ctg}\varphi \times \{\exp(2 \times \theta \times \tan\varphi) - 1\}. \tag{3.18}$$

Thus, energy dissipation in the region OAR during rigid rotation around point O can be expressed in the form

$$D_{AOR} = c \times V_0 \times r_0 \times \operatorname{ctg}\varphi \times \{\exp(2 \times \Theta \times \tan\varphi) - 1\}. \tag{3.19}$$

Although this is the same basic mechanism, the relations for the rotation process shown in Fig.14 are more complicated because of c value variation from one region to another. Therefore the energy dissipation in this case was calculated numerically.

The material tear process along the KD' line is similar to that shown in Fig.13c.

The moment necessary to start a rotation process (Fig.14) can be calculated from the following equation:

$$M_0 \times \omega = M_G \times \omega + M_T \times \omega + D_{OCK}, \tag{3.20}$$

where M_G - moment due to gravity forces, M_T - moment due to the tear process along the KD' line:

$$M_T = 0.5 \times (OD')^2 \times S_{t5} - 0.5 \times (OK)^2 \times S_{t5}, \tag{3.21}$$

D_{OCK} - energy dissipated in the region OCK.

In the case of tool rotation around point C (Fig.14), a material tear along a straight line (for example CH') can be assumed to be a kinematically admissible mechanism. The moment necessary to start such a process can be calculated from the following energy equation:

$$M_c \times \omega = M_T \times \omega - M_G \cdot \omega, \tag{3.22}$$

where M_T - moment due to the tear process for CH' line:

$$M_T = 0.5 \times (CH')^2 \times S_{t2},$$

M_G - moment due to gravity forces.

However, material tear along the BC line ($S_{t3} = 2.94\,\mathrm{kPa}$) turns out to be an energetically most effective mechanism. In that case, a low filling tool volume efficiency of such a process makes it inacceptable for practical use (an analysis similar to that leading to Eqs.(3.8) and (3.10) shows that the material wedge created in region $CBB^{XV}D^{XV}$ does not slide down). So the tool filling process should be realized as rotation around point O.

A more effective tool filling process, from both the energetical point of view and tool volume efficiency can be proposed. This process consists in material sliding along the CH' slip line ($\Omega = \pi/2 - (\alpha + \varphi)$) and then, rotation around point C. In the first part (sliding), material cohesion on the slip line diminishes to the residual value $c = c_R = 3.92$ kPa ($S_t = S_{tR} = 2.94$ kPa) according to Eqs.(3.3) and (3.4). Hence, for the following tool rotation around point C, material tear along the straight line CH' appears to be the energetically most effective kinematically admissible mechanism.

3.2. Solutions for the material obeying the Tresca yield criterion

It seems to be important to point out, that the solution for the layer cutting problem with scale - shaped rigid zones could also be obtained for other types of materials.

Let us consider a rigid-perfectly plastic material obeying the Tresca yield criterion:

(3.23) $$|\tau| = \mathrm{c},$$

and the associated flow rule (2.2). With such an assumption no volume change could be observed and quite good agreement between the theoretical solutions and experimental data was reported. It was assumed that the material cohesion parameter c decreases according to Eqs.(3.3) and $(3.1)_2$ along the slip lines and some characteristic values of the process (Fig.4) are similar to those discussed before ($H = 35$cm, $c_0 = 19.6$kPa, $c_R = 3.92$kPa). As an example, the tool pushing phase (Fig.4a,b) will be discussed.

A kinematically admissible solution with two slip lines BC and CD and a moving rigid triangular zone BCD, as well as the solution after the first step of the process, is presented in Fig.17 (the angles α and ρ are equal to 45°). After the first step of the process one can distinguish two separate material regions: $B''C''D''$ and $C'D'D''C''$ with different material parameter values (the cohesion parameter c decreases according to Eq.$(3.1)_2$). Figures 17–20 illustrate the situation after subsequent steps of the process. The dashed line indicates the configuration before the step and the solid line the configuration after the step. For the CD slip line position before the step a dotted line was used. The configuration after the second step and three different material parameter regions

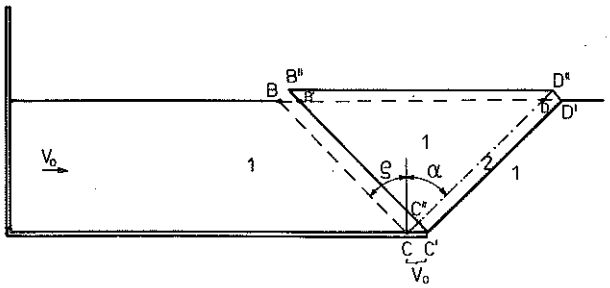

Fig. 17. The kinematically admissible solution at a certain stage of the rigid wall pressure process (for the Tresca yield criterion material) - first step.

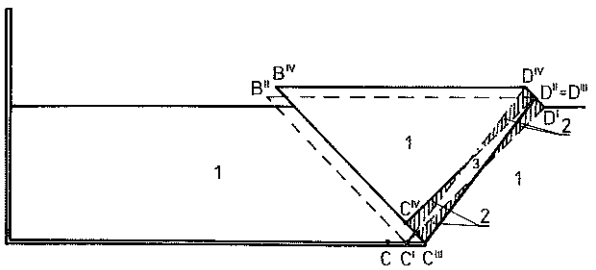

Fig. 18. The kinematically admissible solution at a certain stage of the rigid wall pressure process (for the Tresca yield criterion material).

were presented in Fig.18. The region indicated by "1" consists of the virgin material and $c_1 = c_0 = 19.6$kPa while in the region "2" $c_2 = 4.84$kPa and in the region "3" $c_3 = 4.02$kPa. In Fig.19 the subsequent slip line CD position after the first five steps was presented. At the beginning its orientation became more and more vertical (compare the positions $C^{\mathrm{I}}D^{\mathrm{I}}$, $C^{\mathrm{III}}D^{\mathrm{III}}$, $C^{\mathrm{V}}D^{\mathrm{V}}$, $C^{\mathrm{VII}}D^{\mathrm{VII}}$, $C^{\mathrm{IX}}D^{\mathrm{IX}}$ and the position $C^{\mathrm{XI}}D^{\mathrm{XI}}$ in Fig.20). At the moment shown in Fig.20 the slip line CD jumps rapidly to the position $C^{\mathrm{XIII}}D^{\mathrm{XIII}}$ with orientation equal to the position $C^{\mathrm{I}}D^{\mathrm{I}}$ ($\alpha = 45°$). Next, the region consisting of the virgin material ($KEHF^{\mathrm{II}}$ in Fig.20) is cut off, while the material parameter distribution within the zone, $KF^{\mathrm{II}}\,HJD^{\mathrm{XIV}}\,G^{\mathrm{I}}\,C^{\mathrm{XIV}}$ is rather complicated. From this moment on, the layer cutting process begins to be repeatable.

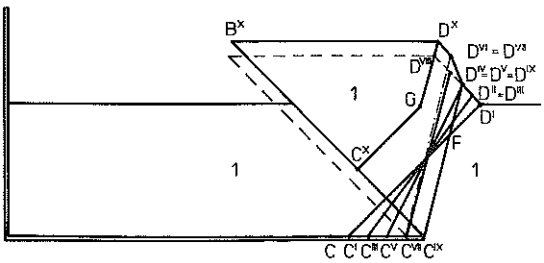

Fig. 19. The kinematically admissible solution at a certain stage of the rigid wall pressure process (for the Tresca yield criterion material) – advanced tool displacement.

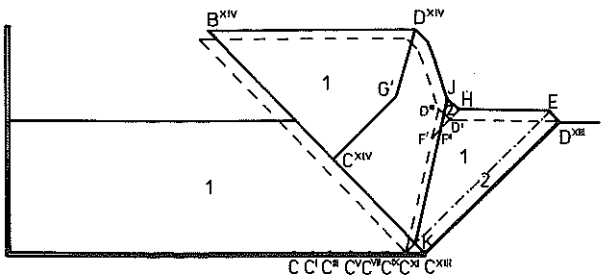

Fig. 20. The kinematically admissible solution at a certain stage of the rigid wall pressure process (for the Tresca yield criterion material) – after advanced tool displacement.

4. Conclusions

It was shown that using quite simple kinematically admissible solutions one can study such a complicated process as that similar to the heavy machine tools working process. Such results cannot be obtained using the characteristics methods or any other simple technique.

Referring to the simple solutions of the theory of plasticity, characteristic scale-shaped rigid zones generated during the cohesive soil cutting process were predicted without any additional assumptions about crack initiations and energetical criteria of propagation.

Although the associated flow rule creates some difficulties as to the interpretation of material dilatation (density in the region 3, Fig.12), in this paper such an assumption was made as the first approximation. Further investigation for such solutions are necessary. On the other hand, a solution with different material parameters within different regions seems to be reasonable for the soil cutting process.

Although it is difficult to assess in this way the complete solutions for such a problem, some advice on how to find more efficient ways of the tool moving process can be given (for example, for the tool filling process).

REFERENCES

1. W.SZCZEPIŃSKI, *Limit states and kinematics of granular media* [in Polish], PWN, 1974.
2. W.SOKOŁOWSKI, *Statics of granular media* [in Polish], PWN, 1958.
3. R.IZBICKI, Z.MRÓZ, *Limit state analysis in mechanics of solids and rocks* [in Polish], PWN, 1976.
4. W.TRĄMPCZYŃSKI, *Mechanics of earth-moving processes as a problem of plasticity theory* [in Polish], Ph.D.-Dissertation, IFTR Rep., 1975.
5. W.TRĄMPCZYŃSKI, *Experimental study of kinetics of soil shoving*, Bull. Acad.Polon. Sci., Série Sci.Techn., **25**, 11, 1977.
6. W.TRĄMPCZYŃSKI, D.SZYBA, *Kinematically admissible solutions for the incipient stage of earth-moving processes in the cases of various pushing wall forms*, Enging. Trans., **39**, 1, 1991.
7. O.ZIENKIEWICZ, K.LUENG, M.PASTOR, *Simple model for transient soil loading in earthquake analysis. Basic model and its application*, Int. J. Num. Anal. Methods Geomech., 19, 453-476, 1985.
8. W.TRĄMPCZYŃSKI, B.PONDER, *Mechanics of earth-moving processes by means of earth work tools* [in Polish], IFTR Rep., 7, 1978.
9. W.SZCZEPIŃSKI, H.WINEK, *Experimental study of granular medium kinetics for certain boundary-value problem*, [in Polish], Rozpr.Inżyn., **20**, 1, 1972.
10. A.DRESCHER, *Application of optically sensitive model materials to the stress analysis in granular media* [in Polish], Mech.Teoret. i Stos., **8**, 4, 1970.
11. B.PAUL, *A modification of the Coulomb-Mohr theory of fracture*, J.Appl.Mech., Trans. ASME, **28**, 1961.
12. J.MACIEJEWSKI, *Incremental analysis of earth-moving mechanisms* [in Polish], M.Sc.-Dissertation, Politechnika Warszawska 1987.
13. T.JESKE, T.PRZEDECKI, B.ROSIŃSKI, *Soil mechanics* [in Polish], PWN, 1966.
14. A.JARZĘBOWSKI, Z.MRÓZ, *On slip and memory rules in the elastic friction contact problems* [in print].

STRESZCZENIE

O PEWNYCH ROZWIĄZANIACH KINEMATYCZNIE DOPUSZCZALNYCH DLA ZAGADNIENIA NAPORU ŚCIAN O KSZTAŁTACH ODPOWIADAJĄCYCH NARZĘDZIOM MASZYN DO ROBÓT ZIEMNYCH

W pracy przedstawiono proste rozwiązania teoretyczne dla zagadnienia przesuwu gruntu wywołanego naporem takich narzędzi maszyn budowlanych, jak łyżka ładowarki. Zakładając sztywno-idealnie plastyczny model ośrodka, którego plastyczność opisuje warunek Coulomba-Mohra oraz stowarzyszone prawo płynięcia, znaleziono rozwiązania kinematyczne problemu. Pokazano, że stosując tę technikę krok po kroku można było opisać tak złożone procesy, jak proces napełniania narzędzia oraz znaleźć bardziej efektywne drogi obciążenia.

Резюме

О НЕКОТОРЫХ КИНЕМАТИЧЕСКИХ ДОПУСТИМЫХ РЕШЕНИЯХ ДЛЯ ПРОБЛЕМЫ НАПОРА СТЕН С ФОРМАМИ ОТВЕЧАЮЩИМИ ИНСТРУМЕНТАМ МАШИН К ЗЕМНЫМ РАБОТАМ

В работе представлены простые теоретические решения для проблемы перемещания грунта, вызванного напором таких инструментов строительных машин как ковш погрузочной машины. Предполагая жестко-идеально пластическую модель среды, пластичность которой описывает условие Кулона-Мора и ассоцированный закон течения, найдены кинематические решения проблемы. Показано, что применяя эту технику шаг за шагом, можно описать так сложные процессы, как процесс наполнения инструмента и найти более эффективные пути нагружения.

POLISH ACADEMY OF SCIENCES
INSTITUTE OF FUNDAMENTAL TECHNOLOGICAL RESEARCH

Received May 8, 1990.